Available online at www.sciencedirect.com
SCIENCE DIRECT®
Fuel 82 (2003) 875–885
FUEL
www.fuelfirst.com

# The initial stage of fuel spray penetration☆

Sergei Sazhin*, Cyril Crua, David Kennaird, Morgan Heikal

*Faculty of Science and Engineering, School of Engineering, University of Brighton, Cockcroft Building, Brighton BN2 4GJ, UK*

Received 14 October 2002; revised 2 December 2002; accepted 3 December 2002; available online 7 January 2003

**Abstract**

Effects of droplet evaporation, break-up and air entrainment on diesel fuel spray penetration have been studied theoretically at the initial stage of spray penetration when the influence of air entrainment is small (up to 0.1–0.2 ms after the start of injection). Theoretical plots of spray penetration versus time are compared with experimental results obtained using an optical single cylinder rapid compression test rig based on a Ricardo Proteus engine. Three models of spray penetration have been compared. In the first, neither break-up nor air entrainment are taken into account. The break-up processes (bag and stripping) are taken into account in the second model, while in the third model both bag break-up and air entrainment processes are considered. It has been found that the agreement between the predictions of the third model with experimental measurements is better than that for the first two models.


*Keywords:* Diesel fuel spray; Two-phase flow; Droplet break-up

## 1. Introduction

The importance of the problem of spray penetration for various applications is well recognized and has been extensively studied experimentally and theoretically [1–5]. A rigorous theory of spray penetration would be very complex as it would need to involve modelling of the formation of ligaments and their break-up, droplet break-up and evaporation, the entrainment of air and the effects of turbulence [6]. A self-consistent modelling of all these processes is still a major challenge. However, this modelling is not always essential for understanding the process and engineering applications. On many occasions it is far more important to establish a 'hierarchy' of the importance of the various processes and develop simplified models suitable for practical applications.

Some work in this direction has been reported in Ref. [7] where simple analytical models describing the initial stage of spray penetration and droplet break-up have been derived. The reduction of droplet size due to break-up has been considered, but an unrealistic assumption, that droplet velocity remains constant, was used. The effects of reduction of droplet size during the penetration process due to effects of evaporation and break-up were ignored. These are taken into account in our present analysis.

Basic equations and approximations are discussed in Section 2. In Section 3 we consider briefly the effect of droplet evaporation on spray penetration. In Sections 4 and 5 the effects of bag and stripping break-up on spray penetration are discussed. A simple schematic presentation of flow and break-up regimes is discussed in Section 6. Some relevant experimental results referring to the initial stage of spray penetration are presented and discussed in Section 7. The main results of the paper are summarised in Section 8.

## 2. Basic equations and approximations

### 2.1. Dynamics of droplets

The initial formation of droplets from a liquid fuel jet has been discussed by a number of authors [8]. For the parameters used in our experiments the Reynolds number is of the order of $10^3$ and the Ohnesorge number is of the order of $10^{-1}$. In this case the expected break-up regime lies between the first wind induced break-up and second wind induced break-up [8]. The contribution of jet in spray penetration process can be ignored as the first approximation

* Corresponding author. Tel.: +44-1273-642677; fax: +44-1273-642301.
*E-mail address:* s.sazhin@brighton.ac.uk (S. Sazhin).
☆ Published first on the web via Fuelfirst.com—http://www.fuelfirst.com

0016-2361/03/$ - see front matter © 2003 Elsevier Science Ltd. All rights reserved.
doi:10.1016/S0016-2361(02)00405-2

in both cases. The initial sizes of droplets will be assumed equal to the nozzle diameter [7].

At the initial stage of spray penetration the analysis can be focused on the equation describing the dynamics of an individual droplet

$$\frac{d^2s}{dt^2} = -\frac{3}{8r} C_D \frac{\rho_g}{\rho_d}\left(\frac{ds}{dt} - v_g\right)\left|\frac{ds}{dt} - v_g\right|, \tag{1}$$

where $s$ is the distance measured from the nozzle, $C_D$ is the drag coefficient, which depends on the Reynolds number $Re = 2\rho_g|v_d - v_g|r/\mu_g$, $\rho_g$ and $\rho_d$ are the gas and droplet density, respectively, $r$ is the droplet's radius, $v_d = (ds/dt)$, $v_g$ is the gas velocity, $t$ is time.

When deriving Eq. (1) it was assumed that the droplet is a perfect sphere. The solution of this equation requires the knowledge of $C_D$ and $v_g$. A number of approximations for $C_D$ has been suggested [1,9–13]. Expressions for $C_D$ suggested by these authors can be used for numerical analysis of Eq. (1), but they are not suitable for analytical estimates, which are sometimes convenient in engineering applications. A much simpler approximation was suggested in Ref. [14] where three ranges of Reynolds numbers were considered: $Re \le 2$ (Stokes flow), $2 < Re \le 500$ (Allen flow) and $500 < Re \le 10^5$ (Newton flow). The functions $C_D(Re)$ for these flows are given by the following expressions: $C_D = 24/Re$ (Stokes flow), $C_D = 18.5/Re^{0.6}$ (Allen flow) $C_D = 0.44$ (Newton flow).

Note that there is an obvious mistake in Ref. [14] where the transition between Stokes and Allen flows was identified with $Re = 0.2$. Predictions of $C_D$ for Stokes and Allen flows match for $Re = 2$ but not for $Re = 0.2$. In the latter case the formula for the Allen flow predicts the values of $C_D$ well below those observed experimentally. The upper value of $Re = 2$ for the Stokes flow is consistent with the results presented in Refs. [15,16], but seems to be larger than follows from the plots presented in Ref. [17]. Although it is sometimes recommended to use $C_D = 24/Re$ for $Re < 0.5$ [15], the error in the prediction of $C_D$ by this formula does not exceed about 20% for $Re < 2$ (see plots in Refs. [15–17]). More accurate expressions for $C_D$ for $Re < 2$ would give the following formulae $C_D = (24/Re)[1 + 3Re/16]^{1/2}$ [14] or $C_D = (24/Re)[1 + Re^{2/3}/6]$ [13]. This mistake in Ref. [14] was overlooked in the authors previous paper [7], but does not change its conclusions.

The expressions for $C_D$ given above do not take into account effects of droplet acceleration, internal circulation, burning, non-spherical shape and vibrations and heating processes. They cannot be applied when Ma is close to or greater than 1 [1,11,18]. The condition $Re < 10^5$ is always satisfied for realistic droplets in diesel engines.

The drag force acting on the droplets leads not only to deceleration of droplets but also to momentum transfer from the droplets to the gas entrained into the spray. The latter process has been discussed in Ref. [19] where the following equation for gas velocity in the near zone of the spray was derived

$$\frac{d}{ds}(\pi r_g^2 v_g^2) = \frac{3\pi r_s^2 \alpha_d}{8r_d} C_D (v_d - v_g)^2, \tag{2}$$

where $r_g$ and $r_s$ are radii of the gas/air jet and the spray itself, respectively, at a certain position $s$, $\alpha_d$ is the volume fraction of droplets in the spray; $r_g$ is usually slightly larger than $r_s$, but as a first approximation we will assume that they both are equal to $s \tan\theta$, $\theta$ is the half angle of the spray cone.

We assume that $v_g$ is so small compared with $v_d$ that its contribution in the right hand side of Eq. (1) can be ignored altogether. Remembering the definitions of $C_D$ for the three types of flow, Eq. (1) can be simplified to:

$$\frac{d^2s}{dt^2} = -\frac{9}{2}\frac{\mu_g}{\rho_d r^2}\frac{ds}{dt} \quad \text{(Stokes flow)}, \tag{3}$$

$$\frac{d^2s}{dt^2} = -\frac{4.577\mu_g^{0.6}\rho_g^{0.4}}{\rho_d r^{1.6}}\left(\frac{ds}{dt}\right)^{1.4} \quad \text{(Allen flow)}, \tag{4}$$

$$\frac{d^2s}{dt^2} = -\frac{0.165\rho_g}{\rho_d r}\left(\frac{ds}{dt}\right)^2 \quad \text{(Newton flow)}. \tag{5}$$

Assuming that $r = \text{const}$. (no evaporation and break-up) the solutions of Eqs. (3)–(5) can be easily found [7]. The effect of air entrainment can be considered as the perturbation to the solutions of Eqs. (3)–(5) [7]

$$\Delta s = \frac{4}{15}\alpha\kappa\sqrt{v_{d0}}t^{5/2} \quad \text{(Stokes flow)}, \tag{6}$$

$$\Delta s = 0.373\kappa v_{d0}^{0.9}\beta t^{5/2} \quad \text{(Allen flow)}, \tag{7}$$

$$\Delta s = 0.533\gamma\kappa v_{d0}^{3/2} t^{5/2} \quad \text{(Newton flow)}, \tag{8}$$

where $v_{d0}$ is the initial droplet velocity, $\kappa = (3r_s^2\alpha_d/8r_d r_{g0})C_D v_{d0}^2$, $\alpha = 9\mu_g/2r_d^2\rho_d$, $\beta = 4.577\mu_g^{0.6}\rho_g^{0.4}/r_d^{1.6}\rho_d$, $\gamma = 0.165\rho_g/r_d\rho_d$, $\Delta s = s_g - s_0$, $s_0$ are the solutions of Eqs. (3)–(5), $s_g$ is the solution of the general Eq. (2). When deriving Eqs. (6)–(8) it was assumed that $|\Delta s| \ll s_0$. In what follows the solutions of Eqs. (3)–(5) will be generalized taking into account the effects of evaporation and droplet break-up.

### 2.2. Evaporation and droplet break-up models

Ignoring the initial stage of droplet evaporation (heat-up period), the time evolution of the droplet's radius in the isothermal approximation can be described by the following equation

$$\frac{dr^2}{dt} = -r_0\mu, \qquad r(0) = r_0 \tag{9}$$

where $\mu = Nu\, k_g(T_g - T_s)/(L\rho_d r_0^3)$ is a constant which does not depend on time, $r_0$ is the initial droplet radius, $Nu$ is the Nusselt number, $k_g$ is the gas thermal conductivity, $T_g$ is the gas temperature, $T_s$ is the temperature of the droplet's surface, $L$ is specific heat of evaporation.

A number of expressions for $Nu$ has been discussed [11,13]. The simplest and the most widely used approximation for this parameter is the following [1]:

$$Nu = 2 + 0.6Re^{1/2}Pr^{1/3}.$$

In the case when $Re$ is small $Nu = 2$ and Eq. (9) can be integrated to give [20]:

$$r = r_0\sqrt{1-\mu t} = r_0\sqrt{1-\frac{2k_g(T_g-T_s)}{L\rho_d r_0^2}t}. \tag{10}$$

A number of droplet break-up models have been suggested [1,8,21–23]. One of the most popular models is based on the comparison between the eigen frequency of droplet oscillations and the frequency of turbulent pulsation in the surrounding gas. This allows the determination of the maximal stable droplet diameter. The predictions of this model are in good agreement with some experimental observations [24].

In our case, however, the driving force of droplet break-up is not the external turbulence, but the kinetic energy of the droplets themselves. In this case a different approach would seem to be more appropriate. As in Ref. [7], this study is based on the model developed in Refs. [25,26] which is particularly attractive for analytical and numerical analysis and is widely used in CFD codes.

In this model two droplet break-up regimes are identified. These are bag break-up when

$$We \equiv \frac{\rho_g v_d^2 r}{\sigma} > 6 \tag{11}$$

and stripping break-up when

$$Z \equiv \frac{We}{\sqrt{Re}} > 0.5, \tag{12}$$

where $We$ is the Weber number, $\sigma$ is the surface tension. The first regime is an analogue of the Rayleigh–Taylor instability accompanied by the development of normal stresses. The second regime is an analogue of the Kelvin–Helmholtz instability accompanied by the development of tangential stresses. The break-up processes described by Eqs. (11) and (12) can take place simultaneously. In this case the dominant process will be determined by the shortest lifetime as described below. Sometimes a more stringent criterion for the stripping instability ($Z > 0.7$) has been used [1]. The modification of our analysis to meet this criterion would be straightforward. It is important not to confuse $Z$ with the Ohnesorge number, $Oh$ [1].

The lifetimes of unstable droplets were estimated as [26]

$$t_b = D\left[\frac{\rho_d r^3}{2\sigma}\right]^{1/2} \quad \text{(bag break-up)} \tag{13}$$

$$t_s = C\frac{r}{v_d}\sqrt{\rho_d/\rho_g} \quad \text{(stripping break-up)}, \tag{14}$$

where $D$ was taken equal to $\pi$ and $C = 13$.

As a first approximation the creation of droplets of different radii during the break-up process was not taken into account. The radii of unstable droplets are allowed to change continuously following the equation:

$$\frac{dr}{dt} = -\frac{r - r_{db(s)}}{t_{b(s)}} \tag{15}$$

where $t_b$ and $t_s$ are defined by Eqs. (13) and (14), respectively, $r_{db(s)}$ are marginally stable radii determined by the conditions $We = 6$ and $Z = 0.5$, respectively. This approximation is justified by the fact that the contribution of smaller droplets generated during the break-up is relatively small and can be ignored. Also, Eq. (15) implies that droplets preserve their spherical shape during the break-up process. The authors appreciate that this is a limitation of the model. Combined solutions of Eq. (15) and Eqs. (3), (4) or (5) for spray penetration for Stokes, Allen and Newton flows will be investigated for the bag and stripping break-up regimes.

## 3. Effect of droplet evaporation

In the case of the Stokes flow Eq. (3) can be simplified to:

$$\frac{d^2s}{dt^2} = -\frac{a_e}{1-\mu t}\frac{ds}{dt}, \qquad a_e = \frac{9}{2}\frac{\mu_g}{\rho_d r_0^2}. \tag{16}$$

Integration of Eq. (16) gives [27]

$$\frac{ds}{dt} = v_{d0}(1-\mu t)^{a_e/\mu},$$
$$s = v_{d0}\frac{1-(1-\mu t)^{(a_e+\mu)/\mu}}{a_e+\mu}, \tag{17}$$

where $v_{d0}$ is the initial velocity of the droplet. The lifetime of evaporating droplets is $t_{ev} = 1/\mu$. During this time the value of $s$ reaches its maximum: $s_{max} = v_{d0}/(a_e + \mu)$.

In the limit of slow evaporation ($\mu \to 0$), the equation for $s$ can be simplified to (cf. Eq. (3) in Ref. [7]):

$$s \approx \frac{v_{d0}}{a_e}[1-(1-\mu t)^{a_e/\mu}]$$
$$= \frac{v_{d0}}{a_e}\left[1 - 1 + \frac{\mu a_e}{\mu}t - \frac{1}{2}\mu^2 t^2\left(\frac{a_e^2}{\mu^2}\right) + \cdots\right]$$
$$= \frac{v_{d0}}{a_e}(1 - e^{-a_e t}).$$

The range of validity of Eq. (17) is defined by the condition:

$$Re = \frac{2\rho_g v_{d0} r_0 (1-\mu t)^{(2a_e+\mu)/2\mu}}{\mu_g} \le 2. \tag{19}$$

If condition (19) is valid at $t = 0$ it will remain valid at all $t > 0$. No simple expressions for spray velocity and spray penetration have been obtained in the case of Allen and Newton flows due to dependence of $\mu$ on $Re$.

## 4. Effect of droplet bag break-up

From Eq. (11) it is obtained:

$$r_{\rm db} = \frac{6\sigma}{\rho_{\rm g} v_{\rm d}^2}. \tag{20}$$

Having substituted Eq. (13) into Eq. (15) the following equation is obtained

$$\frac{{\rm d}r}{{\rm d}t} = -\frac{r - r_{\rm db}}{a_{\rm b} r^{3/2}}, \tag{21}$$

where $a_{\rm b} = D\sqrt{\rho_{\rm d}/(2\sigma)}$. Eq. (21) is valid for $r > r_{\rm db}$. Otherwise $r = {\rm const}$.

Assuming that $r \gg r_{\rm db}$ the right hand side of Eq. (21) can be simplified to $-1/(a_{\rm b}\sqrt{r})$ and the solution can be written as:

$$r = r_0(1 - a_{\rm rb}t)^{2/3}, \qquad a_{\rm rb} = \frac{3}{2a_{\rm b} r_0^{3/2}}. \tag{22}$$

When $r$ approaches $r_{\rm db}$, the term proportional to $r_{\rm db}$ in Eq. (21) can be considered as a perturbation. In this case we can look for the solution of Eq. (21) in the form

$$r = r_{\rm l} + \Delta r, \tag{23}$$

where $r_{\rm l}$ is defined by Eq. (22), $|\Delta r| \ll r_{\rm l}$.

The combination of Eqs. (21)–(23) gives

$$\frac{{\rm d}\Delta r}{{\rm d}t} = \frac{1}{2a_{\rm b} r_0^{3/2}(1 - a_{\rm rb}t)}\Delta r + \frac{r_{\rm db}}{a_{\rm b} r_0^{3/2}(1 - a_{\rm rb}t)}, \tag{24}$$

where $r_{\rm db}(t)$ is defined by Eq. (20). The solution of this equation gives:

$$\Delta r = -2r_{\rm db}\left[1 - (1 - a_{\rm rb}t)^{-1/2a_{\rm b}a_{\rm rb}r_0^{3/2}}\right]. \tag{25}$$

We took into account that $\Delta r(t = 0) = 0$. The time limit is determined by the conditions $r \gg r_{\rm db}$ and $t < a_{\rm rb}^{-1}$. Eq. (25) contains the unknown function $r_{\rm db}(t)$ which depends on droplet velocity and cannot be explicitly calculated. In the limiting case when $r \to r_{\rm db}$ we have ${\rm d}r/{\rm d}v_{\rm d} \to 0$ (the trajectory in the $(r, v_{\rm d})$ space is perpendicular to the $r$-axis). $r = {\rm const}$ at $r < r_{\rm db}$. In this case the solution of Eqs. (3)–(5) reduces to the one considered in Ref. [7].

The solution of Eq. (21) was investigated under the assumption that the velocity of droplets is constant [7]. In this section this assumption is relaxed but the restriction $r \gg r_{\rm db}$ will be imposed.

### 4.1. Stokes flow

Having substituted Eq. (22) into Eq. (3) we obtain

$$\frac{{\rm d}^2 s}{{\rm d}t^2} = -\frac{a_{\rm e}}{(1 - a_{\rm rb}t)^{4/3}}\frac{{\rm d}s}{{\rm d}t}, \tag{26}$$

where $a_{\rm e}$ is the same as in Eq. (16).

Integration of Eq. (26) gives

$$\frac{{\rm d}s}{{\rm d}t} = v_{\rm d0}\exp\left[-a_{\rm vb}\left(\frac{1}{(1 - a_{\rm rb}t)^{1/3}} - 1\right)\right], \tag{27}$$

$$s = \frac{a_{\rm vb}^3 v_{\rm d0}}{a_{\rm rb}}\exp(a_{\rm vb})\left[\frac{1}{2}\left(E_1(a_{\rm vb}) - E_1\left(\frac{a_{\rm vb}}{(1 - a_{\rm rb}t)^{1/3}}\right)\right)\right.$$
$$+\exp\left(-\frac{a_{\rm vb}}{(1 - a_{\rm rb}t)^{1/3}}\right)\left[-\frac{1 - a_{\rm rb}t}{a_{\rm vb}} + \frac{(1 - a_{\rm rb}t)^{2/3}}{2a_{\rm vb}^2}\right.$$
$$\left.\left.-\frac{(1 - a_{\rm rb}t)^{1/3}}{2a_{\rm vb}} - \exp(-a_{\rm vb})\left[-\frac{1}{a_{\rm vb}^3} + \frac{1}{2a_{\rm vb}^2} - \frac{1}{2a_{\rm vb}}\right]\right]\right], \tag{28}$$

where

$$E_1(z) = \int_z^\infty \frac{{\rm e}^{-t}}{t}{\rm d}t, \quad a_{\rm vb} = \frac{3a_{\rm e}}{a_{\rm rb}}.$$

The conditions for the validity of these equations can be presented as:

$$r_0(1 - a_{\rm rb}t)^{2/3} \gg \frac{6\sigma}{\rho_{\rm g} v_{\rm d0}^2}\exp\left[\frac{6a_{\rm e}}{a_{\rm rb}}\left(\frac{1}{(1 - a_{\rm rb}t)^{1/3}} - 1\right)\right] \tag{29}$$
(condition: $r \gg r_{\rm db}$)

$$r_0(1 - a_{\rm rb}t)^{2/3} < \frac{\mu_{\rm g}}{\rho_{\rm g} v_{\rm d0}}\exp\left[\frac{3a_{\rm e}}{a_{\rm rb}}\left(\frac{1}{(1 - a_{\rm rb}t)^{1/3}} - 1\right)\right] \tag{30}$$
(Stokes flow: $Re < 2$).

### 4.2. Allen flow

Dividing Eq. (4) by Eq. (21), taken in the limit $r \gg r_{\rm db}$, we obtain

$$\frac{{\rm d}v_{\rm d}}{{\rm d}r} = \frac{b_{\rm e} r_0^{1.6} a_{\rm b} v_{\rm d}^{1.4}}{r^{1.1}}, \tag{31}$$

where $b_{\rm e} = \beta(r_0)$.

Integration of Eq. (31) gives:

$$v_{\rm d} = \frac{{\rm d}s}{{\rm d}t} = \frac{v_{\rm d0}}{\left[1 + 4b_{\rm e} r_0^{1.6} v_{\rm d0}^{0.4} a_{\rm b}\left(\frac{1}{r^{0.1}} - \frac{1}{r_0^{0.1}}\right)\right]^{2.5}}$$
$$= \frac{v_{\rm d0}}{\left[1 + 4b_{\rm e} r_0^{1.5} v_{\rm d0}^{0.4} a_{\rm b}\left(\frac{1}{(1 - a_{\rm rb}t)^{1/15}} - 1\right)\right]^{2.5}}. \tag{32}$$

The conditions for the validity of these equations can be presented as:

$$r_0(1 - a_{\rm rb}t)^{2/3} \gg \frac{6\sigma}{\rho_{\rm g} v_{\rm d0}^2}\left[1 + 4b_{\rm e} r_0^{1.5} v_{\rm d0}^{0.4} a_{\rm b}\left(\frac{1}{(1 - a_{\rm rb}t)^{1/15}} - 1\right)\right]^5 \tag{33}$$
(condition: $r \gg r_{\rm db}$)

$$\frac{\mu_g}{\rho_g v_{d0}}\left[1+4b_e r_0^{1.5} v_{d0}^{0.4} a_b\left(\frac{1}{(1-a_{rb}t)^{1/15}}-1\right)\right]^{2.5} \le r_0(1-a_{rb}t)^{2/3} < \frac{250\mu_g}{\rho_g v_{d0}}\left[1+4b_e r_0^{1.5} v_{d0}^{0.4} a_b\left(\frac{1}{(1-a_{rb}t)^{1/15}}-1\right)\right]^{2.5}$$

(Allenflow: $2 \le Re < 500$). (34)

### 4.3. Newton flow

Having substituted Eq. (22) into Eq. (5) we obtain:

$$\frac{d^2 s}{dt^2} = -\frac{c_e}{(1-a_{rb}t)^{2/3}}\left(\frac{ds}{dt}\right)^2, \qquad c_e = \frac{0.165\rho_g}{\rho_d r_0}. \tag{35}$$

Integration of Eq. (35) gives:

$$\frac{ds}{dt} = v_{d0}\left[1 - \frac{3c_e v_{d0}[(1-a_{rb}t)^{1/3}-1]}{a_{rb}}\right]^{-1}, \tag{36}$$

$$s = \frac{1}{c_e}\left\{\frac{(1-a_{rb}t)^{2/3}-1}{2} + \frac{(1-a_{rb}t)^{1/3}-1}{\beta_N} + \frac{1}{\beta_N^2}\ln\left|\frac{\beta(1-a_{rb}t)^{1/3}-1}{\beta_N - 1}\right|\right\}, \tag{37}$$

where

$$\beta_N = \frac{3c_e v_{d0}}{a_{rb} + 3c_e v_{d0}}$$

In the limit of small $a_{rb}$ (no break-up), Eq. (37) reduces to Eq. (5) of Ref. [7].

The conditions for the validity of these equations can be presented as:

$$r_0(1-a_{rb}t)^{2/3} \gg \frac{6\sigma}{\rho_g v_{d0}^2}\left[1 - \frac{3c_e v_{d0}[(1-a_{rb}t)^{1/3}-1]}{a_{rb}}\right]^2 \quad \text{(condition : } r \gg r_{db}\text{)}. \tag{38}$$

$$r_0(1-a_{rb}t)^{2/3} \ge \frac{250\mu_g}{\rho_g v_{d0}}\left[1 - \frac{3c_e v_{d0}[(1-a_{rb}t)^{1/3}-1]}{a_{rb}}\right] \quad \text{(Newton flow : } Re \ge 500\text{)}. \tag{39}$$

## 5. Effect of droplet stripping break-up

From Eq. (12) it is obtained:

$$r_{ds} = \frac{b_s}{v_d^3}, \qquad b_s = \frac{\sigma^2}{2\rho_g\mu_g}. \tag{40}$$

The combination of Eqs. (14), (15) and (40) gives

$$\frac{dr}{dt} = -\frac{r v_d - \frac{b_s}{v_d^2}}{c_s r}, \tag{41}$$

where $c_s = C\sqrt{\rho_d/\rho_g}$. Eq. (41) is valid for $r > r_{ds}$. Otherwise $r = \text{const}$.

Assuming that $r \gg r_{ds}$ the right hand side of Eq. (41) can be simplified to $-v_d/c_s$. The contribution of the term proportional to $b_s$ can be studied similarly to Section 4. In contrast to the case of bag break-up this equation cannot be solved unless we know the time dependence of $v_d$.

### 5.1. Stokes flow

Division of Eq. (3) by Eq. (41) taken for $r \gg r_{ds}$ gives:

$$\frac{dv_d}{dr} = \frac{a_e r_0^2 c_s}{r^2}. \tag{42}$$

This equation can be integrated to give:

$$v_d = v_{d0} + a_e r_0^2 c_s\left(\frac{1}{r_0} - \frac{1}{r}\right). \tag{43}$$

Having substituted the latter equation into Eq. (41) taken for $r \gg r_{ds}$ and integrating the latter equation we obtain

$$t = \frac{r_0 - r}{\alpha_s} + \frac{\beta_s}{\alpha_s^2}\ln\left|\frac{\beta_s - \alpha_s r_0}{\beta_s - \alpha_s r}\right|, \tag{44}$$

where

$$\alpha_s = \frac{v_{d0}}{c_s} + a_e r_0; \qquad \beta_s = a_e r_0^2.$$

The combination of Eqs. (43) and (44) gives an implicit expression for droplet velocity. The integration of Eq. (41) taken for $r \gg r_{ds}$ gives:

$$r = r_0 - s/c_s. \tag{45}$$

The combination of Eqs. (44) and (45) gives an implicit expression for droplet penetration. The range of applicability of these equations can be determined similarly to the case of bag break-up.

### 5.2. Allen flow

The combination of Eqs. (4) and (41) taken for $r \gg r_{ds}$ gives:

$$v_d = v_{d0}\left[1 - \frac{b_e r_0^{1.6} c_s}{v_{d0}^{0.6}}\left(\frac{1}{r^{0.6}} - \frac{1}{r_0^{0.6}}\right)\right]^{5/3}. \tag{46}$$

The combination of Eqs. (5) and (46) taken for $r \gg r_{ds}$ gives:

$$t = -\frac{c_s}{v_{d0}}\int_{r_{d0}}^{r} \frac{dr}{\left[1 - \frac{b_e r_{d0}^{1.6} c_s}{v_{d0}^{0.6}}\left(\frac{1}{r^{0.6}} - \frac{1}{r_0^{0.6}}\right)\right]^{5/3}}. \tag{47}$$

Eqs. (45)–(47) give an implicit expression for droplet velocities and penetration. The range of applicability of these equations can be determined similarly to the case of bag break-up.

### 5.3. Newton flow

The combination of Eqs. (5) and (41) taken for $r \gg r_{ds}$ gives

$$v_d = v_{d0}\left(\frac{r}{r_0}\right)^{c_e r_0 c_s}, \tag{48}$$

or

$$r = r_0\left(\frac{v_d}{v_{d0}}\right)^{1/(c_e r_0 c_s)}, \tag{49}$$

where $c_e$ is the same as in Eq. (35).

Having substituted Eq. (49) into Eq. (5) we obtain:

$$\frac{dv_d}{dt} = -c_e v_{d0}^{1/(c_e r_{d0} c_s)} v_d^{(2c_e r_{d0} c_s - 1)/(c_e r_{d0} c_s)}. \tag{50}$$

If $(2c_e r_{d0} c_s - 1)/(c_e r_{d0} c_s) \neq 1$ then Eq. (50) can be integrated to give:

$$v_d = \frac{v_{d0}}{\left[1 + c_e v_{d0}\left(1 - \frac{1}{c_e r_{d0} c_s}\right)t\right]^{c_e r_{d0} c_s/(c_e r_{d0} c_s - 1)}}. \tag{51}$$

If $(2c_e r_{d0} c_s - 1)/(c_e r_{d0} c_s) = 1$ then Eq. (50) can be integrated to give:

$$v_d = v_{d0}\exp(-c_e v_{d0} t). \tag{52}$$

When deriving Eq. (52) we took into account that the condition $(2c_e r_{d0} c_s - 1)/(c_e r_{d0} c_s) = 1$ is satisfied when $r_{d0} = 1/(c_e c_s)$. Integration of Eqs. (51) and (52) gives:

$$s = r_{d0} c_s\left\{1 - \left[\frac{1}{1 + c_e v_{d0}\left(1 - \frac{1}{c_e r_{d0} c_s}\right)t}\right]^{1/(c_e r_{d0} c_s - 1)}\right\}, \tag{53}$$

$$s = \frac{1}{c_e}[1 - \exp(-c_e v_{d0} t)]. \tag{54}$$

Eq. (53) is valid when $r_{d0} \neq 1/(c_e c_s)$. Otherwise, Eq. (54) needs to be used.

## 6. Schematic presentation of flow and break-up regimes

In the previous sections a number of approximate solutions referring to different types of flow and different break-up mechanisms have been presented. At the same time the analysis presented so far does not allow us to recognize, in an easy way, the situation to which each equation may be applied. This is clarified in this section. The values of velocities and droplet radii for which the Stokes, Allen and Newton flow approximations are valid will be clearly identified. Also, the regions of bag and stripping break-ups will be identified. Then the characteristic times for droplet evaporation, and bag and stripping instabilities will be compared for typical values of fuel droplets and gas parameters in diesel engines.

The applicability of approximations of Stokes, Allen and Newton flows is determined by the values of $Re$. Let $Re_i$ be threshold values between Stokes and Allen flows ($Re_1 = 2$), Allen and Newton flows ($Re_2 = 500$) and the upper limit of the Newton flow ($Re_3 = 10^5$).

The boundaries between these flows are determined by the equation:

$$v_d = \frac{\mu_g Re_i}{2 r \rho_g}. \tag{55}$$

Taking the decimal logarithm on both sides of Eq. (55) we can rewrite it as

$$\log v_d = a_{fi} - \log r, \tag{56}$$

where $a_{fi} = \log(\mu_g Re_i/2\rho_g)$, both $v_d$ and $r$ are dimensional (SI units).

In a similar way, from Eqs. (20) and (40) the thresholds for bag and stripping break-ups can be presented as

$$\log v_d = a_{thb} - \frac{1}{2}\log r, \tag{57}$$

$$\log v_d = a_{ths} - \frac{1}{3}\log r, \tag{58}$$

where

$$a_{thb} = \log\sqrt{\frac{6\sigma}{\rho_g}}, \qquad a_{ths} = \frac{1}{3}\log\left[\frac{\sigma^2}{2\rho_g\mu_g}\right].$$

Using the same values of parameters for sprays as in Ref. [7]: $\rho_g = 19.7\ \mathrm{kg/m^3}$, $\mu_g/\rho_g = 3.3 \times 10^{-6}\ \mathrm{m^2/s}$, $\sigma = 21.8 \times 10^{-3}\ \mathrm{N/m}$, we obtain: $a_{f1} = -5.48$; $a_{f2} = -3.08$; $a_{f3} = -0.78$; $a_{thb} = -1.09$; $a_{ths} = -0.24$. Since the dependence of these parameters on $\rho_g$, $\mu_g$ and $\sigma$ is rather weak, these values can be considered as typical for practical applications.

The plots of $\log v_d$ versus $-\log r$ for these values of parameters are presented in Fig. 1. Since all plots on this diagram are straight lines, they can be easily adjusted to any other combination of input parameters.

Typical droplet radii in diesel fuel sprays are greater than $10^{-6}$ m and their velocities are greater than 1 m/s. In this case, as follows from Fig. 1, the Stokes flow approximation is generally not applicable to the analysis of sprays in engines. At $r > 10^{-5}$ m the threshold velocities for the stripping break-up are higher than for the bag break-up. The opposite takes place for $r < 10^{-5}$ m. The range of applicability of the conditions $r \gg r_{db}$ and $r \gg r_{ds}$ can be checked by showing that the point on the diagram corresponding to $v_d$ and $r$ under consideration is not close to the threshold lines for bag and stripping instabilities.

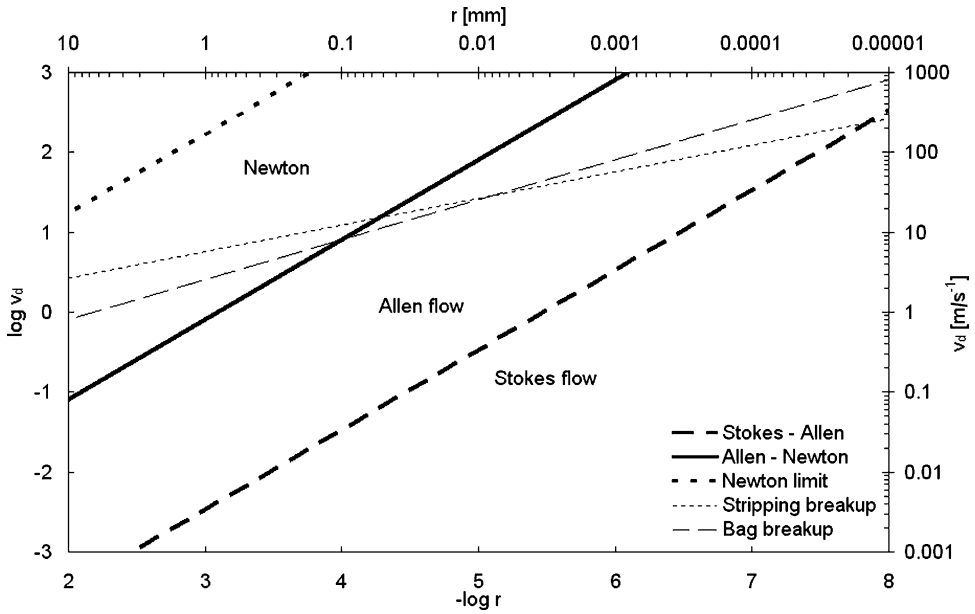


Fig. 1. Threshold values of droplet velocities and droplet radii corresponding to transition from Stokes to Allen flow; Allen to Newton flow and the threshold value of applicability of the Newton flow approximation. Threshold values of droplet velocities versus droplet radii corresponding to the development of stripping break-up and bag break-up. The following values of parameters have been taken for calculation of the lines: $\rho_d = 760$ kg/m$^3$, $v_d = 318.3$ m/s, $L = 2.5 \times 10^5$ J/kg, $k_g = 0.061$ W/(m K), $T_s = 300$ K and $T_g = 880$ K [20].

Other parameters which need to be taken into account when deciding the applicability of the approximations discussed in the previous sections are the lifetimes of unstable droplets ($t_b$ and $t_s$), defined by Eqs. (13) and (14), and the evaporation time $t_{ev} = \mu^{-1}$ (see Eq. (9)). From Eqs. (13), (14) and (9) we have

$$\log t_b = b_{thb} + \frac{3}{2}\log r, \tag{59}$$

$$\log t_s = b_{ths} + \log r, \tag{60}$$

$$\log t_{ev} = b_{th(ev)} + 2\log r, \tag{61}$$

where

$$b_{thb} = \log\left[\frac{D\sqrt{\rho_d}}{\sqrt{2\sigma}}\right], \qquad b_{ths} = \log\left[\frac{C}{v_d}\sqrt{\frac{\rho_d}{\rho_g}}\right],$$

$$b_{th(ev)} = \log\left[\frac{L\rho_d}{2k_g(T_g - T_s)}\right],$$

all parameters are in SI units ($t$ and $r$ are dimensional).

Taking the same numerical values of parameters as before, and $\rho_d = 760$ kg/m$^3$, $v_d = 318.3$ m/s, $L = 2.5 \times 10^5$ J/kg, $k_g = 0.061$ W/(m K), $T_s = 300$ K and $T_g = 880$ K [20], we obtain the following numerical values: $b_{thb} = 2.618$, $b_{ths} = -0.596$, $b_{th(ev)} = 6.429$.

Plots of $\log t_i$ versus $-\log r$ are shown in Fig. 2, where $t_i = t_b, t_s$ or $t_{ev}$. As follows from this figure, for $r < 0.01$ μm $t_{ev}$ is smaller than $t_b$ and $t_s$. This means that the evaporation is the dominant process for these radii and the contribution of droplet break-up can be ignored. For $r > 1$ μm $t_s$ is smaller than $t_b$ and $t_{ev}$. This means that for droplets with these radii the dominant process which needs to be accounted for is stripping break-up. Plots similar to those shown in Fig. 2 can be presented for other values of parameters (e.g. temperatures of gas and droplets and droplet velocities).

## 7. Experimental results

### 7.1. Experimental set-up

The experimental set-up is a rapid compression machine based on a single cylinder Ricardo Proteus test engine converted to two-stroke cycle operation by the addition of inlet and exhaust ports in the cylinder liner. The inlet and exhaust valves were removed to increase the room available in the cylinder head for optical access. An optical chamber 50 mm in diameter and 80 mm in length was fitted between the cylinder and head to enable a developed spray to be visualised. Four removable sapphire glass windows provided optical access to the combustion chamber, with a viewable area approximately 30 mm wide and 60 mm high. The nominal speed was 500 rpm, and in order to further increase the volume available for the optical chamber the compression ratio was reduced to 9:1. The intake air was conditioned to provide a near quiescent environment with in-cylinder temperatures and pressures up to 720 K and 12 MPa, respectively [28], corresponding to a real engine compression ratio of 19:1.

A second generation Bosch common rail system was used with a maximum rail pressure of 160 MPa. To ensure a stable rail pressure with minimal fluctuation, the fuel pump

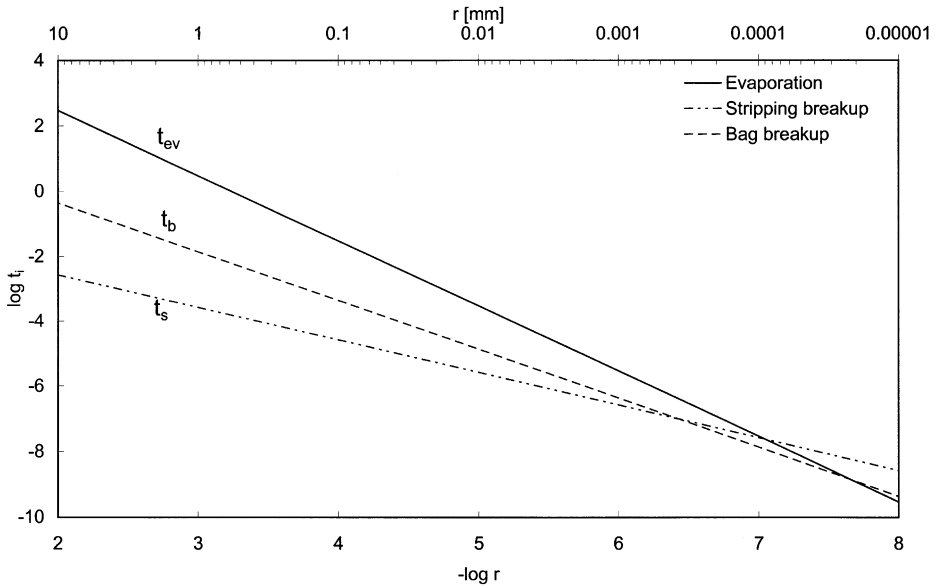


Fig. 2. Plots of $t_{ev}$, $t_b$ and $t_s$ versus $-\log r$ for the same values of parameters as in Fig. 1.

was powered by an electric motor running at 1400 rpm. The rail and delivery pipe were both instrumented with pressure transducers, and the pipe from the rail to the injector was kept short, representative of a real vehicle system. A fuel injection equipment (FIE) controller was developed [28] to enable independent control of injection characteristics (timing, duration, pressure). The custom controller allowed control of initial needle drive current and PID control of the fuel rail pressure.

The nozzle used for this study was a single-hole mini-sac orifice type, with a hole diameter of 200 μm and an equivalent cone angle of 130° [29]. The nozzle hole was manufactured by conventional spark erosion technique and then micro-honed by hydro grinding so that an entry radius and surface finish representative of a production nozzle were obtained. The needle was of the single-guided type and was fitted with a Hall effect needle lift sensor. The nozzle and controller were calibrated on a Moewald test bed and the nozzle delivery rates were measured using a Lucas rate gauge. The diesel fuel had a cetane number of 55, a density of 837 kg/m$^3$, and a sulphur content of 0.026% by mass.

A high-speed CCD video camera operating at 27,000 frames per second was used to record spray injections, with a resolution of 128 × 64 pixels × 256 grey levels. The camera was triggered by a dedicated signal emitted by the custom-built FIE controller and synchronised to the injection pulse.

Sprays were side lit using a halogen lamp as shown in Fig. 3. Liquid spray tip penetration lengths were measured manually at each video frame. The variation in penetration lengths was found to be ±4% from the average curve. The camera resolution was measured to be 0.3 mm per pixel. Hence, the overall uncertainty was estimated to be ±6%. The sensitivity of the imaging technique on droplet concentration was not measured, but laser scattering tests of the liquid spray showed that the droplet dispersion at the spray tip was low. Therefore, it is believed that the droplet density gradients at the tip of the spray are particularly high, and that the limited sensitivity of the camera did not result in significant errors in measured spray tip penetration lengths.

The time delay between the actual start of injection pulse and the start of the video recording was assessed by using a light-emitting diode (LED) linked to the injector pulse signal and positioned within the field of view of the camera. It was found that the start of the video recordings and the start of the injection pulse (as represented by the LED) matched. It is therefore concluded that these two events have been separated by less than 0.04 ms (exposure time for 1 frame), and can be assumed coincident. The times at which the first fuel droplets were seen leaving the nozzle were measured to be 0.60, 0.45 and 0.37 ms after the start of the recording for injection pressures of 60, 100 and

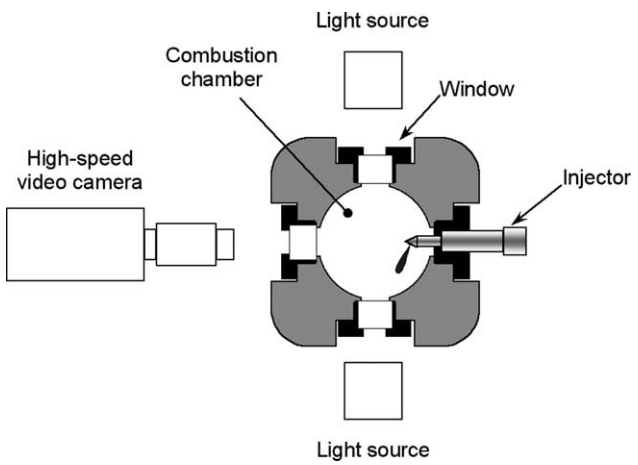


Fig. 3. Experimental set-up for high-speed video recording of spray evolution.

160 MPa, respectively. The data presented here have been adjusted to compensate for this delay.

### 7.2. Results

Spray penetration lengths were measured for injection pressures in the range from 60 to 160 MPa and ambient densities in the range from 25 to 56 kg/m$^3$. The in-cylinder temperature at top dead centre was calculated to be 570 K. It is expected that fuel evaporation should be minimal at that temperature. The results of measurements were compared with the predictions of the models taking into account bag and stripping break-up processes. The range of parameters used allowed us to identify the droplet dynamics with the Newton regime and use the results presented in Sections 4.3 and 5.3. Evaporation effects were negligibly small in our experiment. The results of the comparison are shown in Figs. 4 and 5 for various gas and injection pressures. The plots are presented using the following approximations: no break-up and air entrainment are taken into account; break-up processes (bag and stripping) are taken into account, but not air entrainment; bag break-up and entrainment processes, based on Eqs. (6)–(8), are taken into account. In the case of air entrainment it was assumed that $\alpha_d = 0.001$ for the first three sets of plots and $\alpha_d = 0.002$ for the last set of plots. This choice of $\alpha_d$ provided the best agreement between experimental results and theoretical plots.

All the plots are presented in the range of validity of the models: $r \gg r_{db(s)}$ (approximated as $r \geq 3.3 r_{db(s)}$) and $t < a_{rb(s)}^{-1}$. As follows from our estimates, the range of validity of the stripping break-up model (about 0.05–0.1 ms) is noticeably narrower than that of the bag break-ups model (about 0.25 ms). Hence the plots are presented in two time ranges: 0–0.1 and 0–0.3 ms for stripping and break-up models for clarity. Since the bag break-up model has a wider range of validity, the effect of air entrainment will be investigated for this model.

As can be seen from Figs. 4 and 5, in all cases presented the simplest model (no break-up and air entrainment) clearly underestimates the observed spray penetration lengths. Taking into account the effects of break-up alone increases the deviation between the theoretical curves and experimental points even further. Good agreement between theoretical and experimental plots are achieved only when both effects of break-up and air entrainment are accounted for. This result could be expected. Air entrainment leads to increase of spray penetration, while the break-up process tends to decrease it. Hence these effects tend to compensate each other. The model is not valid at times greater than about 0.1–0.2 ms when the two phase flow approximation needs to be used [7].

Although the trends, similar to those shown in Figs. 4 and 5, are typical for a number of other combinations of parameters, in some cases the agreement between

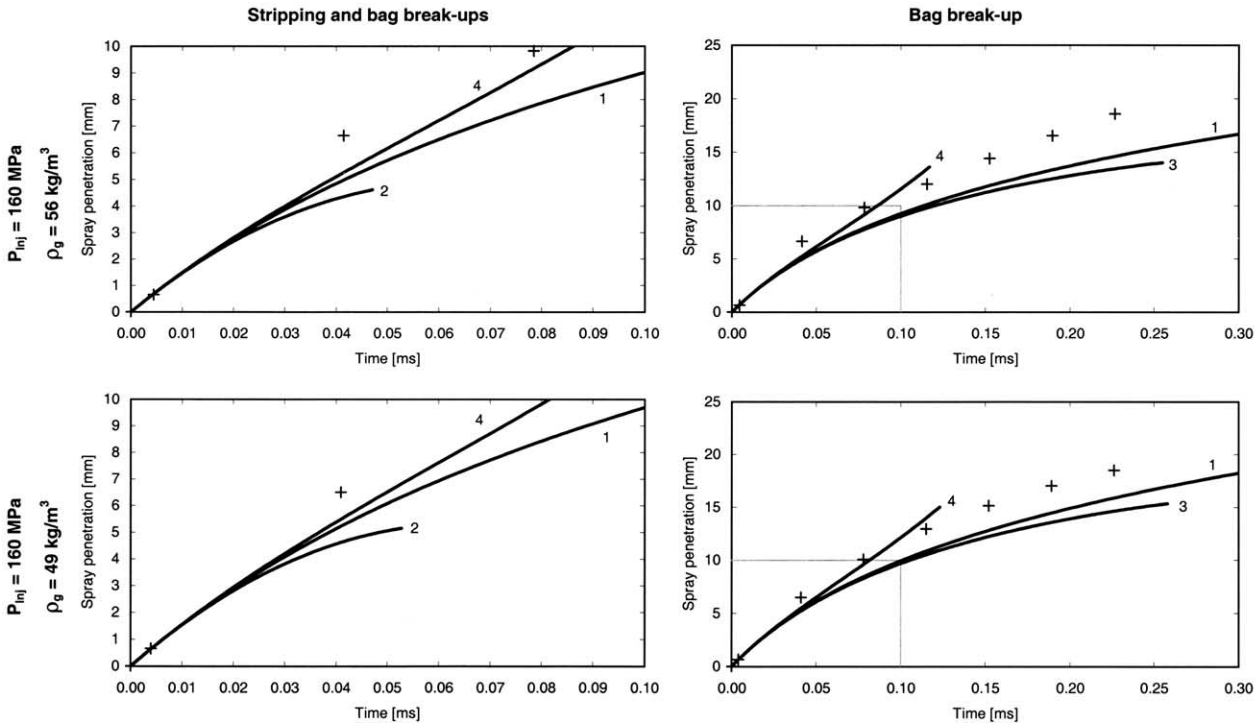


Fig. 4. Comparison between measured spray penetration lengths (+) and theoretically predicted spray penetration lengths in the cases when no break-up and air entrainment are taken into account (curves 1); stripping break-up process is taken into account (curves 2); bag break-up process is taken into account (curves 3); bag break-up and entrainment processes are taken into account (curves 4). Upper curves refer to $P_{inj} = 160$ MPa and $\rho_g = 56$ kg/m$^3$; lower curves refer to $P_{inj} = 160$ MPa and $\rho_g = 49$ kg/m$^3$. Left and right sets of curves refer to different ranges of time intervals. The stripping break-up curves are shown only on the left plots while bag break-up curves are shown on the right plots.

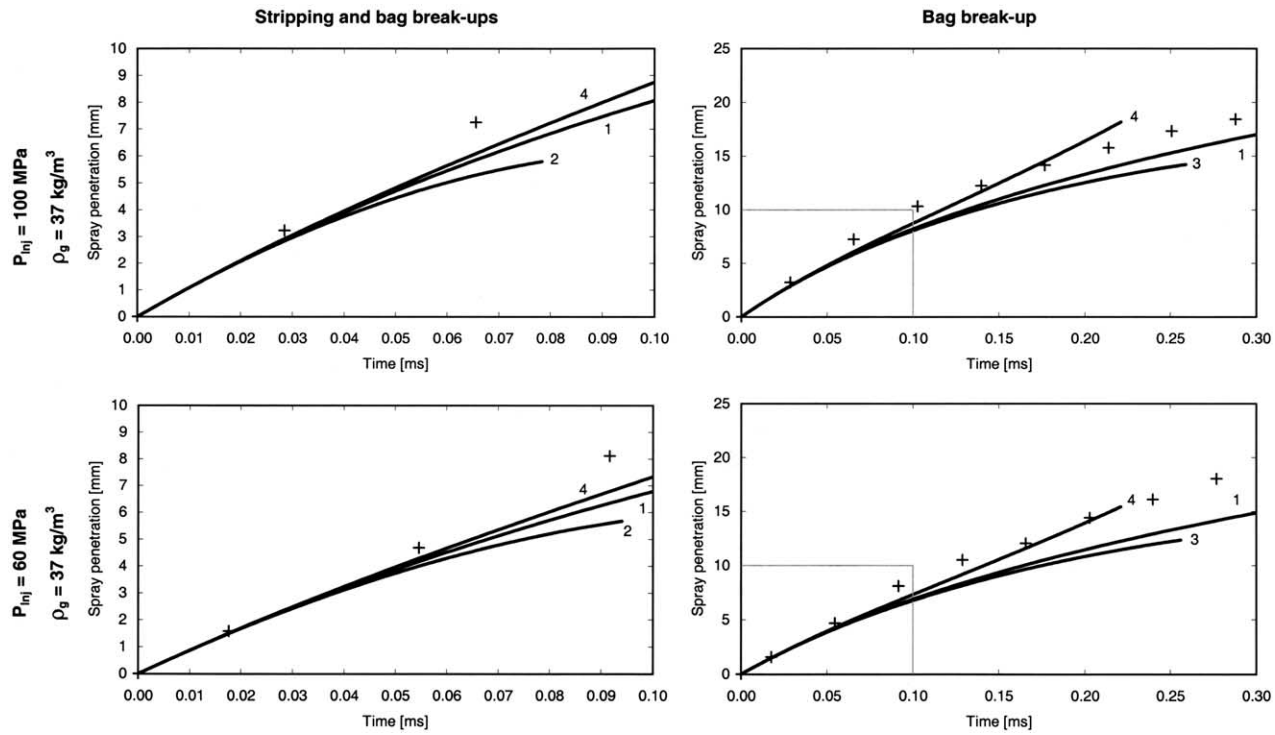


Fig. 5. Comparison between measured spray penetration lengths (+) and theoretically predicted spray penetration lengths in the cases when no break-up and air entrainment are taken into account (curves 1); stripping break-up process is taken into account (curves 2); bag break-up process is taken into account (curves 3); bag break-up and entrainment processes are taken into account (curves 4). Upper curves refer to $P_{inj} = 100$ MPa and $\rho_g = 37$ kg/m$^3$; lower curves refer to $P_{inj} = 60$ MPa and $\rho_g = 37$ kg/m$^3$. Left and right sets of curves refer to different ranges of time intervals. The stripping break-up curves are shown only on the left plots while bag break-up curves are shown on the right plots.

theoretical plots and experimental points turned out to be less convincing (e.g. in the case when $P_{inj} = 160$ MPa and $\rho_g = 37$ kg/m$^3$, and $P_{inj} = 160$ MPa and $\rho_g = 25$ kg/m$^3$). Further investigation is required to understand the reason for this deviation.

## 8. Conclusions

Effects of droplet evaporation, break-up and air entrainment on spray penetration have been studied theoretically in three regimes: Stokes, Allen and Newton flows. The formulae for spray penetration obtained are valid at the initial stage of spray penetration when the effects of air entrainment are negligible. Theoretical plots have been compared with spray penetration measured experimentally using the single cylinder Ricardo Proteus test engine. For the values of parameters observed in this experiment the flow regime has been identified with the Newton flow. The contributions of Stokes and Allen flows at the final stages of spray penetration have not been significant. The comparison has been performed for three models: no break-up and air entrainment are taken into account (simplest model); break-up processes (bag and stripping) are taken into account, but not air entrainment; bag break-up and air entrainment processes are taken into account. It has been shown that the first two models do not give good agreement with experimental measurements, while the agreement between the predictions of the third model with experimental measurements has been reasonably good. All models are expected to be valid during about 0.1–0.2 ms after start of injection.

## Acknowledgements

The authors are grateful to Dr L. Dombrovsky for discussion of the draft version of this paper and Ricardo Consulting Engineers for technical and financial support. EPSRC loan pool is acknowledged for providing access to equipment used in gathering data.

## References

[1] Borman GL, Ragland KW. Combustion engineering. New York: McGraw-Hill; 1998.
[2] Loth E. Numerical approaches for motion of dispersed particles, droplets and bubbles. Prog Energy Combust Sci 2000;26:161–223.
[3] Hentschel W. Optical diagnostics for combustion process development of direct-injection gasoline engines. Proc Combust Inst 2000;28:1119–35.
[4] Iyer VA, Abraham J, Magi V. Exploring injected droplet size effects on steady liquid penetration in a diesel spray with a two-fluid model. Int J Heat Mass Transfer 2002;45:519–31.

[5] Pozorski J, Sazhin SS, Wacławczyk M, Crua C, Kennaird D, Heikal M. Spray penetration in a turbulent flow. Flow Turbul Combust 2002; 68:153–65.
[6] Faeth GM, Hsiang L-P, Wu P-K. Structure and breakup properties of sprays. Int J Multiphase Flow 1995;21(Suppl):99–127.
[7] Sazhin SS, Feng G, Heikal MR. A model for fuel spray penetration. Fuel 2001;80:2171–80.
[8] Lefebvre AH. Atomization and sprays. London: Taylor & Francis; 1989.
[9] Wallis GB. One-dimensional two-phase flows. New York: McGraw-Hill; 1969.
[10] Morsi SA, Alexander AJ. An investigation of particle trajectories in two-phase flow systems. J Fluid Mech 1972;55:193–208.
[11] Yanenko NN, Soloukhin RI, Papyrin AN, Fomin VM. Supersonic two-phase flows with non-equilibrium particle velocities. Novosibirsk: Nauka Publishing House; 1980. in Russian.
[12] Panton RL. Incompressible flow. New York: Wiley; 1996.
[13] Feng Z-G, Michaelides EE. Heat and mass transfer coefficients of viscous spheres. Int J Heat Mass Transfer 2001;44:4445–54.
[14] Douglas JF, Gasiorek JM, Swaffield JA. Fluid mechanics. London: Longman; 1995.
[15] Robertson JA, Crowe CT. Engineering fluid mechanics, 6th ed. New York: Wiley; 1997. p. 438.
[16] White FM. Fluid mechanics, 4th ed. New York: McGraw-Hill; 1999. p. 457.
[17] Munson BR, Young DF, Okiishi TH. Fundamentals of fluid mechanics, 4th ed. New York: Wiley; 2002. p. 582.
[18] Levich VG. Physicochemical hydrodynamics. NJ: Prentice-Hall; 1962.
[19] Ghosh S, Hunt JCR. Induced air velocity within droplet driven sprays. Proc R Soc Lond 1994;A444:105–27.
[20] Sazhin SS, Feng G, Heikal MR, Goldfarb I, Goldshtein V, Kuzmenko G. Thermal ignition analysis of a monodisperse spray with radiation. Combust Flame 2001;124:684–701.
[21] Shraiber AA, Podvysotsky AM, Dubrovsky VV. Deformation and breakup of drops by aerodynamic forces. Atomization Sprays 1996;6: 667–92.
[22] Chigier N, Reitz RD. Regimes of jet breakup and breakup mechanisms (physical aspects). In: Kuo Kenneth K, editor. Recent advances in spray combustion: spray atomization and drop burning phenomena. American Institute of Aeronautics and Astronautics, Inc; 1998. p. 109–35.
[23] Lin SP. Regimes of jet breakup and breakup mechanisms (mathematical aspects). In: Kuo Kenneth K, editor. Recent advances in spray combustion: spray atomization and drop burning phenomena. American Institute of Aeronautics and Astronautics, Inc; 1998. p. 137–60.
[24] Sevik M, Park SH. The splitting of drops by turbulent fluid flow. ASME J Fluid Engng 1973;95:53–60.
[25] Reitz RD, Diwakar R. Effect of drop breakup on fuel sprays. SAE report 860469; 1986.
[26] Reitz RD, Diwakar R. Structure of high-pressure fuel sprays. SAE report 870598; 1987.
[27] Demirtzi D. Spray penetration taking into account the influence of droplet evaporation. The Final Year Project Report. The University of Brighton; 2001.
[28] Kennaird DA, Crua C, Heikal M, Morgan R, Bar F, Sapsford S. A new high pressure diesel spray research facility. Proceedings of the Conference on Computational and Experimental Methods in Reciprocating Engines, Professional Engineering Publishing Limited; 2000. p. 179–88.
[29] Kennaird DA, Crua C, Lacoste J, Heikal M, Gold MR, Jackson NS. In-cylinder penetration and break-up of diesel sprays using a common-rail injection system. SAE publication 2002-01-1626; 2002.